Geochemical Perspectives Letters

Experimental evidence for fluid-induced melting in subduction zones

G. Rustioni[1], A. Audétat[1], H. Keppler[1*]

OPEN ACCESS

doi: 10.7185/geochemlet.1925

Abstract

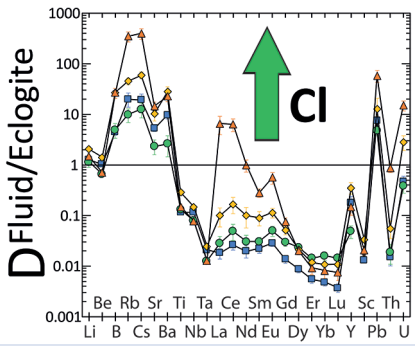

Although subduction zones are the main source of seismic and volcanic hazards on Earth, the causes of melting in volcanic arcs are still not fully understood. Recent models suggested that melting in the mantle wedge is not caused by hydrous fluids, but by sediment melts ascending from the subducted slab. A main argument for these models was that hydrous fluids are "too dilute" to produce the trace element enrichment observed in arc magmas. Here we demonstrate experimentally that even moderate salinities enhance the partitioning of trace elements such as the light rare earths, alkalis, alkaline earths, Pb, and U into the fluid by several orders of magnitude. Our data therefore show that saline hydrous fluids released from the basaltic part of the oceanic crust may produce the enrichment in LILE and light REE elements, and the negative Nb-Ta anomaly observed in typical arc magmas.

Received 7 June 2019 | Accepted 28 August 2019 | Published 22 October 2019

Introduction

In subduction zones, oceanic crust is recycled into the mantle. Thermal models show that the temperature of the mantle wedge above the subducting slab is actually considerably lower than in other parts of the shallow upper mantle (Syracuse *et al.*, 2010). Melting must therefore be caused by other effects, most likely by the addition of water, which may reduce the melting temperatures of mantle peridotite by several 100 °C (Kawamoto and Holloway, 1997; Gaetani and Grove, 1998). Water may be transferred from the subducted oceanic slab to the mantle wedge in the form of aqueous fluids, released by the dehydration of hydrous minerals, or by sediment melts. Already early studies (Perfit *et al.*, 1980; Arculus and Powell, 1986) noted that the trace element enrichment pattern in magmas from volcanic arcs above a subduction zone is distinctly different from that observed in magmas at divergent plate boundaries, *e.g.*, mid-ocean ridges. Typical features of arc magmas include high enrichments of large ion lithophile elements (LILE, such as Rb^{+}, Cs^{+}, Sr^{2+}, Ba^{2+}) and light rare earth elements (REE, such as La^{3+} and Ce^{3+}), but strong depletions of high field strength elements (HFSE, such as Ti^{4+}, Nb^{5+} and Ta^{5+}). Some experimental studies (Kessel *et al.*, 2005; Hermann *et al.*, 2006) suggested that trace element transport by aqueous fluids is unable to produce the observed trace element enrichment pattern in arc magmas. This led to the suggestion that sediment melts are the main agents of metasomatism in the mantle wedge above subduction zones (Kelemen *et al.*, 2005; Hermann *et al.*, 2006; Skora and Blundy, 2010; Behn *et al.*, 2011; Spandler and Pirard, 2013). Previous studies, however, did not consider the effect of chloride, which may affect the partition behaviour of various trace elements by the formation of chloride complexes in the fluid. As the subducted oceanic crust was in contact with seawater, it is expected to contain chloride and measurements of the Cl/H_2O ratio of primitive arc magmas (Métrich and Wallace, 2008), as well as other lines of evidence (Kawamoto *et al.*, 2013), are consistent with the incorporation of aqueous fluids (Manning, 2004) containing up to 15 wt. % NaCl. In the present study, we therefore for the first time directly measured the effect of chlorine on the partitioning of trace elements between aqueous fluids and the minerals of the subducted basaltic crust at conditions corresponding to the typical depth of the slab below the volcanic front.

Methods

Experiments were carried out in an end-loaded piston cylinder apparatus (Boyd and England, 1960) at 4 GPa and 800 °C with run durations between 2 and 7 days. Synthetic MORB (mid-ocean ridge basalt) glass doped with a suite of trace elements was loaded together with water or NaCl solutions into platinum capsules. A layer of diamond powder was inserted in the middle of the capsule between the layers of MORB powder to provide some empty pore space between the diamond grains for trapping the fluid (Ryabchikov *et al.*, 1989). After quenching of the experiments, the sample capsules were cooled to liquid nitrogen temperature and cut in half. Both the compositions of the minerals and of the quenched fluid trapped between the diamond grains were then measured

1. Bayerisches Geoinstitut, Universität Bayreuth, 95440 Bayreuth, Germany
* Corresponding author (email: hans.keppler@uni-bayreuth.de)

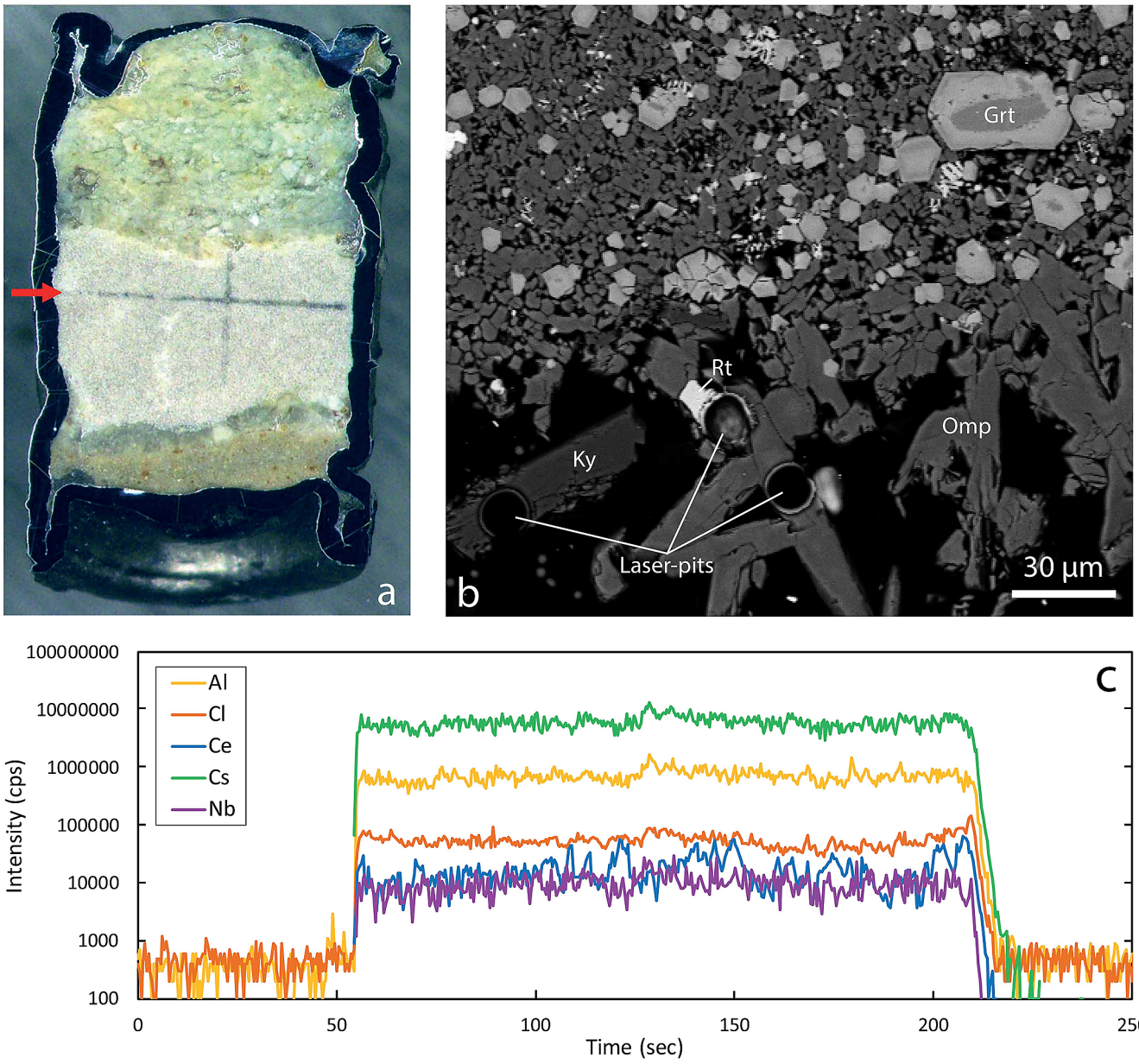

Figure 1 Run products from high pressure experiments. **(a)** Cross section of a sample capsule after an experiment (image width 5 mm). A white layer of diamond powder is sandwiched between the silicate sample. The red arrow points to a laser ablation trace. **(b)** Backscatter electron image of the silicate part of a sample, consisting mostly of omphacite (Omp) and garnet (Grt) with minor kyanite (Ky) and rutile (Rt). In the centre of some garnet crystals, remnants of the garnet seeds are visible. **(c)** Laser ablation analysis of frozen fluid in the diamond trap, demonstrating the homogeneity of the sample.

in frozen state (Kessel *et al.*, 2005) by laser ablation ICP-MS. Additional details about the experimental and analytical methods are given in the Supplementary Information.

Results and discussion

During the high pressure experiments, the glasses recrystallised to an eclogitic assemblage of omphacite, garnet, rutile, and kyanite, *i.e.* the same minerals that are expected to be stable in the subducted basaltic oceanic crust below the volcanic arc (Fig. 1). Other accessory phases likely do not occur in natural MORB at eclogite facies conditions. The solubility of phosphorus in garnet is so high that apatite and other phosphates are unlikely to form (Konzett and Frost, 2009). Due to the very low K_2O content in natural MORB, eclogites of MORB composition either contain no phengite at all or at most traces of this mineral (*e.g.*, Okrusch *et al.*, 1991; see also the Supplementary Information for further discussion). Indeed, in sub-solidus experiments with natural MORB at 3 GPa and 800 °C, Carter *et al.* (2015) did not observe any phengite or apatite.

Mineral compositions in our experiments were found to be uniform in the entire sample, consistent with attainment of equilibrium throughout the entire charge. With a few exceptions, as discussed below, laser ablation ICP-MS analyses of trace element concentrations yielded homogeneous compositions of both the quenched fluid phase and the minerals (see Fig. 1 for typical laser ablation signals). Fluid/mineral partition coefficients $D^{fluid/mineral} = c^{fluid}/c^{mineral}$ were calculated from the measured trace element concentrations in fluid (c^{fluid}) and coexisting minerals ($c^{mineral}$). Bulk fluid/eclogite partition coefficients were then calculated from the individual fluid/mineral partition coefficients assuming an eclogitic mineralogy with 59 % omphacite, 39 % garnet and 2 % rutile. Experimental details,

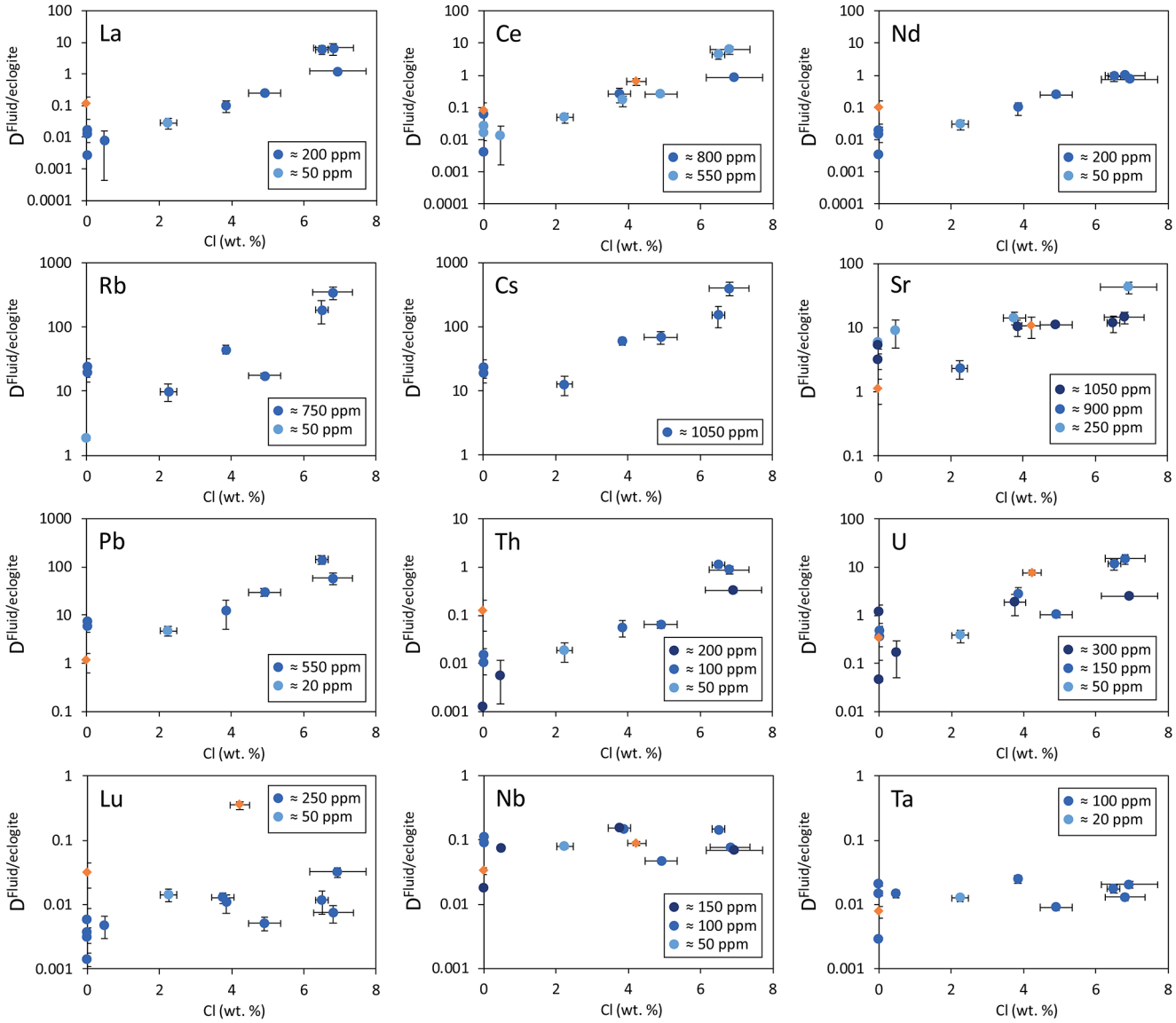

Figure 2 Effect of chloride on fluid/eclogite partition coefficients of trace elements at 4 GPa and 800 ˚C. Blue data points are the results from "forward" experiments, where the trace elements were initially doped into the solid starting material, while orange data points are from "reversed" experiments, which started with all trace elements dissolved in the fluid. For the forward experiments, results for different initial trace element concentrations in the starting material are given. Error bars are one standard deviation. Data for these and additional elements are given in Tables S-1 to S-8.

compositions of all phases and calculated bulk fluid eclogite partition coefficients are compiled in Tables S-1 to S-8 of the Supplementary Information.

A major problem in all studies of element partitioning between minerals and fluid is attainment of equilibrium, since the diffusion coefficients of most of the relevant trace elements in the minerals are very low. In order to circumvent this problem, we introduced periodic temperature fluctuations by ±30 ˚C in our experiments, which enhanced grain growth and equilibration by Ostwald ripening (*i.e.* the dissolution of smaller grains at higher temperature and the growth of larger grains upon cooling). Indeed, the resulting grain sizes observed after runs with these sinusoidal temperature fluctuations were generally much larger than for experiments at constant temperature, but mineral compositions were not affected. In order to demonstrate conclusively the attainment of equilibrium, we also performed some reversed experiments, starting with a trace element-free MORB glass and trace element-doped solutions. In general, both the normal "forward" experiments starting with trace element-doped MORB glass and the reversed experiments gave very consistent results. We are therefore confident that the trace element partition coefficients reported here represent true chemical equilibrium between aqueous fluid and minerals. Moreover, results from experiments with different concentration levels of trace elements yielded consistent partition coefficients, implying that Henry´s law is fulfilled.

Figure 2 shows the fluid/eclogite partition coefficients for some selected trace elements as a function of the chloride content in the fluid. For the light rare earths, such as La and Ce, there is a striking increase of $D^{fluid/eclogite}$ by up to three orders of magnitude even for moderate salinities (up to 15 wt. % NaCl). Similar, although smaller effects are seen for the alkalis (*e.g.*, Rb and Cs) and the alkaline earths (Sr). Pb, Th, and U also show striking increases with salinity. On the other hand, both the typical high field strength elements, such as Nb and Ta as well as the heavy rare earth (*e.g.*, Lu) appear to be unaffected by chloride.

Our data for Cl-free aqueous fluids are generally consistent with those from a previous study (Kessel *et al.*, 2005), as shown in Figure 3. For saline fluids, there are no published data

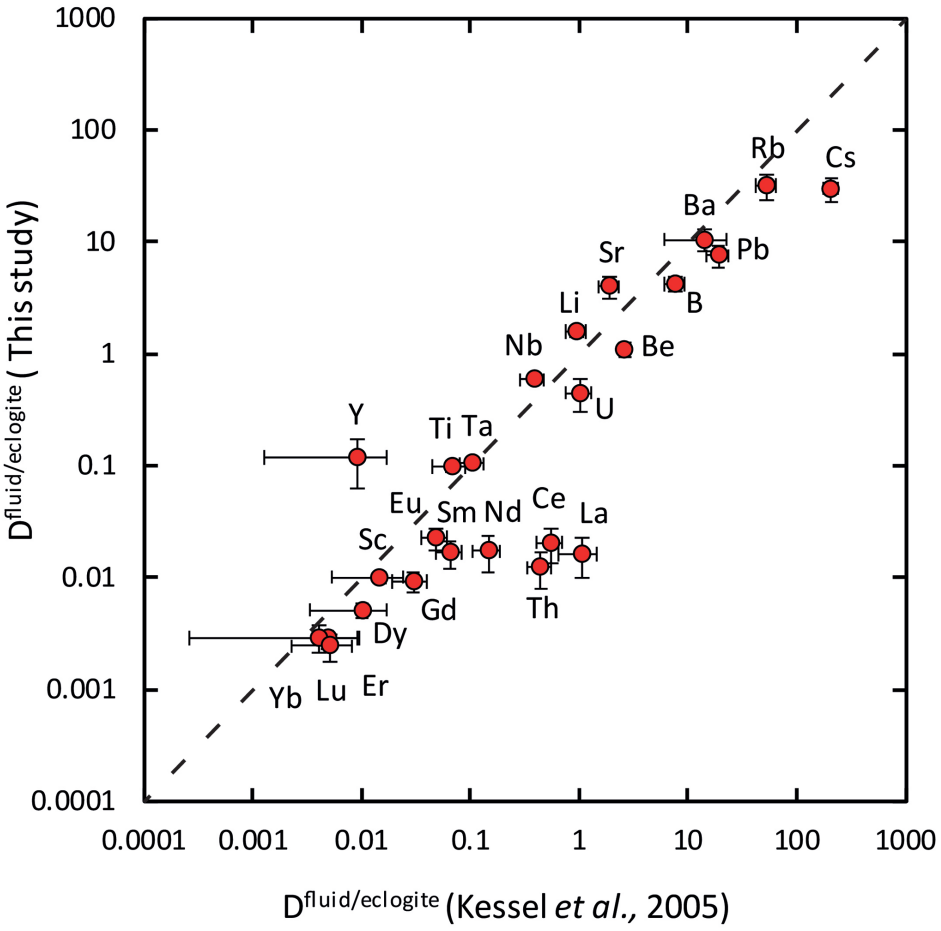

Figure 3 Comparison of the fluid/eclogite partition coefficients for Cl-free fluids measured in this study with those reported by Kessel *et al.* (2005). Both sets of experiments were carried out at 4 GPa and 800 ˚C, with a bulk composition resembling MORB.

that could be directly compared with our results. However, both studies on mineral solubilities (Bali *et al.*, 2011; Tropper *et al.*, 2011; Tsay *et al.*, 2014) and fluid/melt partitioning (Keppler, 1996; Kawamoto *et al.*, 2014) at lower pressures suggest that those elements that are affected by fluid salinity indeed form stable chloride complexes in aqueous fluids. In particular, Tsay *et al.* (2014) noted an increase of the solubility of $La_2Si_2O_7$ and $Nd_2Si_2O_7$ in aqueous fluid by one order of magnitude upon addition of 1.5 M NaCl at 800 ˚C and 2.6 GPa. The formation of chloride complexes will tend to stabilise the trace element in the fluid and therefore increase the fluid/eclogite partition coefficient. Only the sensitivity of Th to chloride is unexpected, as it behaves differently from other HFSE trace elements, such as Nb and Ta. However, the ionic radius of Th^{4+} is significantly larger than that of Nb^{5+}, Ta^{5+}, or Ti^{4+}, such that its geochemical behaviour may be transitional between a typical high field strength and a large ion lithophile element. We also tried to measure the fluid/eclogite partitioning of Zr and Hf, two important HFSE trace elements, but here we encountered experimental problems. The distribution of these elements in the quenched fluid inside the diamond trap was always highly inhomogeneous, which precluded the reliable determination of fluid concentrations and partition coefficients. A possible reason could be the very low solubility (Bernini *et al.*, 2013) of zircon $ZrSiO_4$ and hafnon $HfSiO_4$, which may have precipitated early during the experiment inside the diamond trap and may have failed to reach equilibrium.

Figure 4 shows the trace element enrichment pattern in the fluid phase from the fluid/eclogite partitioning experiments as a function of salinity. An important observation here is that a pure aqueous fluid would not be able to produce all of the trace element enrichment features observed in arc magmas. While such fluids may effectively transport some large ion lithophile elements, like Rb, Cs, Sr, and Ba (with fluid/eclogite partition coefficients >1), the light rare earths as well as uranium would be retained in the eclogite. This used to be one of the main arguments why aqueous fluids were considered to be "too dilute" to produce the trace element enrichment observed in arc magmas and why alternative mechanisms, such as metasomatism by sediment melt were proposed. However, for elevated salinities the enrichment pattern in aqueous fluid has a striking similarity to that observed in arc magmas, with the light rare earths and U becoming mobile in the fluid together with the large ion lithophile elements, while at the same time, high field strength elements, such as Nb, Ta, and Ti are nearly completely retained in the eclogite. The high Ba/La, Ba/Nb, and U/Th ratios match well with those inferred from primitive arc basalts (see Supplementary Information for further discussion). In particular, the "negative Nb-Ta anomaly" *i.e.* the strong depletion of Nb and Ta relative to both light rare earths and large ion lithophile elements is a hallmark of subduction zone magmas. Saline fluids can fractionate these elements by three orders of magnitude, mainly through the effect of Cl on rare earth partitioning. In a chloride-free system, the fluid/eclogite partition coefficient of La and Ce could be increased to a similar value by a temperature increase of several 100 ˚C, ultimately leading to melting (Kessel *et al.*, 2005). However, in silicate melts, Nb and Ta would also become mobile and therefore, this effect cannot produce the negative Nb Ta anomaly observed in subduction zone magmas.

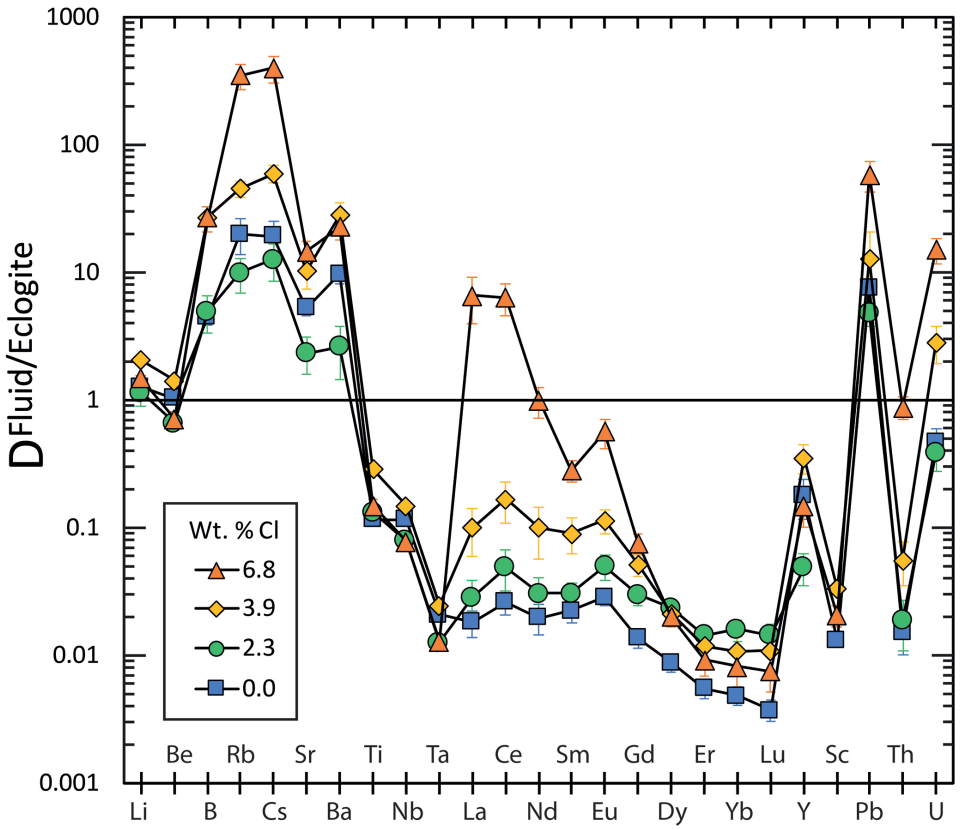

Figure 4 Trace element enrichment patterns in fluids from fluid/eclogite partitioning experiments at 4 GPa and 800 ˚C. Error bars are one standard deviation. Data for these and additional elements are given in Tables S-1 to S-8.

Conclusions

Our experimental data show that saline fluids released from the basaltic layer of the subducted slab can account for most features in the trace element enrichment pattern observed in subduction zone magmas. In the light of these experiments, the relative importance of aqueous fluids and sediment melts in the formation of arc magmas needs to be reconsidered. Strong evidence for the involvement of sedimentary material comes from isotopic data; already Armstrong (1971) noted a close correlation between the $^{206}Pb/^{204}Pb$ ratio of arc magmas and the sediments in front of some arcs and similar evidence has been presented for different isotope systems. However, these observations do not necessarily require the involvement of sediment melts. The isotopic signal observed may also have been transported by aqueous fluids; our data suggest that both Pb and Sr may be efficiently transported by saline fluids (Fig. 4) and even Be and Nd may be significantly mobile under some conditions. High Th/La ratios in arc magmas may be inherited from sediments (Plank, 2005); however, it remains uncertain whether sediment melts could effectively transport these elements, as they are strongly retained in residual monazite and other phases and the fractionation of Th and La between melt and monazite may not always operate in the right direction (Skora and Blundy, 2010). On the other hand, experimental data suggest that mantle metasomatism by sediment melts produces distinctly potassic melts (Mallik *et al.*, 2015) different from average subduction zone magmas. Thermal models of subduction zones (Syracuse *et al.*, 2010) suggest temperatures below the arc that are lower than those required for dehydration melting (*e.g.*, Mann and Schmidt, 2015). Higher temperatures have been inferred from Ce/H_2O ratios. However, the Ce/H_2O geothermometer (Plank *et al.*, 2009) is based on the assumption that the Ce/H_2O ratio in fluids and melts is a function of temperature only. Our data (Fig. 2) show that at the same temperature, this ratio may vary by three orders of magnitude as a function of salinity.

Acknowledgements

We thank Patrick O´Brien for discussing some aspects of eclogite mineralogy with us. Reviews by Matthieu Galvez and by an anonymous referee helped to improve the manuscript. This work was supported by the DFG International Research Training Group "Deep Earth Volatile Cycles" (GRK 2156/1).

Editor: Cin-Ty Lee

Additional Information

Supplementary Information accompanies this letter at http://www.geochemicalperspectivesletters.org/article1925.

Cite this letter as: Rustioni, G., Audétat, A., Keppler, H. (2019) Experimental evidence for fluid-induced melting in subduction zones. *Geochem. Persp. Let.* 11, 49–54.

References

Arculus, R.J., Powell, R. (1986) Source component mixing in the regions of arc magma generation. *Journal of Geophysical Research* 91, 5913–5926.

Armstrong, R.L. (1971) Isotopic and chemical constraints on models of magma genesis in volcanic arcs. *Earth and Planetary Science Letters* 12, 37–142.

Bali, E., Audetat, A., Keppler, H. (2011) The mobility of U and Th in subduction zone fluids: an indicator of oxygen fugacity and fluid salinity. *Contributions to Mineralogy and Petrology* 161, 597–613.

Behn, M.D., Kelemen, P.B., Hirth, G., Hacker, B.R., Massonne, H.J. (2011) Diapirs as the source of the sediment signature in arc lavas. *Nature Geoscience* 4, 641–646.

Bernini, D., Audetat, A., Dolejs, D., Keppler, H. (2013) Zircon solubility in aqueous fluids at high temperatures and pressures. *Geochimica et Cosmochimica Acta* 119, 178–187.

Boyd, F.R., England, J.L. (1960) Apparatus for phase-equilibrium measurements at pressures up to 50 kilobars and temperatures up to 1750°C. *Journal of Geophysical Research* 65, 741–748.

Carter, L.B., Skora, S., Blundy, J.D., De Hoog, J.C.M., Elliott, T. (2015) An experimental study of trace element fluxes from subducted oceanic crust. *Journal of Petrology* 56, 1585–1606.

Gaetani, G.A., Grove, T.L. (1998) The influence of water on melting of mantle peridotite. *Contributions to Mineralogy and Petrology* 131, 323–346.

Hermann, J., Spandler, C., Hack, A., Korsakov, A.V. (2006) Aqueous fluids and hydrous melts in high-pressure and ultra-high pressure rocks: Implications for element transfer in subduction zones. *Lithos* 92, 399–417.

Kawamoto, T., Holloway, P.R. (1997) Melting temperature and partial melt chemistry of H_2O-saturated mantle peridotite to 11 gigapascals. *Science* 276, 240–243.

Kawamoto, T., Yoshikawa, M., Kumagai, Y., Mirabueno, M.H.T., Okuno, M., Kobayashi, T. (2013) Mantle wedge infiltrated with saline fluids from dehydration and decarbonation of subducting slab. *Proceedings of the National Academy of Sciences of the USA* 110, 9663–9668.

Kawamoto, T., Mibe, K., Bureau, H., Reguer, S., Mocuta, C., Kubsky, S., Thiaudiere, D., Ono, S., Kogiso, T. (2014) Large-ion lithophile elements delivered by saline fluids to the sub-arc mantle. *Earth, Planets and Space* 66, doi:10.1186/1880-5981-66-61.

Kelemen, P.B., Hanghøj, K., Greene, A.R. (2005) One view of the geochemistry of subduction-related magmatic arcs, with an emphasis on primitive andesite and lower crust. In: Rudnick, R.L. (Ed.) *Treatise of Geochemistry, Volume 3, The Crust*. Elsevier, Amsterdam, 593–659.

Keppler, H. (1996) Constraints from partitioning experiments on the composition of subduction-zone fluids. *Nature* 380, 237–240.

Kessel, R., Schmidt, M.W., Ulmer, P., Pettke, T. (2005) Trace element signature of subduction-zone fluids, melts and supercritical liquids at 120–180 km depth. *Nature* 437, 724–727.

Konzett, J., Frost, D.J. (2009) The high P-T stability of hydroxyl-apatite in natural and simplified MORB – an experimental study to 15 GPa with implications for transport and storage of phosphorus and halogens in subduction zones. *Journal of Petrology* 50, 2043–2062.

Mallik, A., Nelson, J., Dasgupta, R. (2015) Partial melting of fertile peridotite fluxed by hydrous rhyolitic melt at 2-3 GPa: implications for mantle wedge hybridization by sediment melt and generation of ultrapotassic magmas in convergent margins. *Contributions to Mineralogy and Petrology* 169, Article Number 48.

Mann, U., Schmidt, M.W. (2015) Melting of pelitic sediments at subarc depths: 1. Flux vs. fluid-absent melting and a parameterization of melt productivity. *Chemical Geology* 404, 150–167.

Manning, C.E. (2004) The chemistry of subduction zone fluids. *Earth and Planetary Science Letters* 223, 1–16.

Métrich, N., Wallace, P.J. (2008) Volatile abundances in basaltic magmas and their degassing paths tracked by melt inclusions. *Reviews in Mineralogy and Geochemistry* 69, 363–402.

Okrusch, M., Matthes, S., Klemd, R., O'Brien P.J., Schmidt, K. (1991) Eclogites at the north-western margin of the Bohemian Massif: A review. *European Journal of Mineralogy* 3, 707–730.

Perfit, M.R., Gust, D.A., Bence, A.E., Arculus, R.J., Taylor, S.R. (1980) Chemical characteristics of island-arc basalts - implications for mantle sources. *Chemical Geology* 30, 227–256.

Plank, T. (2005) Constraints from thorium/lanthanum on sediment recycling at subduction zones and the evolution of the continents. *Journal of Petrology* 46, 921–944.

Plank, T., Cooper, L.B., Manning, C.E. (2009) Emerging geothermometers for estimating slab surface temperatures. *Nature Geoscience*, 2, 611–615.

Ryabchikov, I.D., Orlova, G.P., Kalenchuk, G.Y., Ganeyev, I.I., Udovkina, N.G., Nosik, L.P. (1989) Reactions of spinel lherzolite with H_2O-CO_2 fluids at 20 kbar and 900 °C. *Geochemistry International* 26, 56–62.

Skora, S., Blundy, J. (2010) High-pressure hydrous phase relations of radiolarian clay and implications for the involvement of subducted sediment in arc magmatism. *Journal of Petrology* 51, 2211–2243.

Spandler, C., Pirard, C. (2013) Element recycling from subducting slabs to arc crust: A review. *Lithos* 170-171, 208–223.

Syracuse, E.M., Van Keken, P.E., Abers, G.A. (2010) The global range of subduction zone thermal models. *Physics of the Earth and Planetary Interiors* 183, 73–90.

Tropper, P., Manning, C.E., Harlov, D.E. (2011) Solubility of $CePO_4$ monazite and YPO_4 xenotime in H_2O and H_2O–NaCl at 800 °C and 1 GPa: Implications for REE and Y transport during high-grade metamorphism. *Chemical Geology* 282, 58–66.

Tsay, A., Zajacz, Z., Sanchez-Valle, C. (2014) Efficient mobilization and fractionation of rare-earth elements by aqueous fluids upon slab dehydration. *Earth and Planetary Science Letters* 398, 101–112.

Geochemical Perspectives Letters

Experimental evidence for fluid-induced melting in subduction zones

G. Rustioni, A. Audétat, H. Keppler

Supplementary Information

The Supplementary Information includes:

- Starting Materials and Methods
- Supplementary Discussion
- Supplementary Tables S-1 to S-8
- Supplementary Information References

Starting Materials and Methods

Starting Materials

Two glasses with K-free average MORB composition were synthesised at 1600 °C. The first one (MORB1) was prepared without trace elements and was used in the reversed experiments. For some forward experiments, part of MORB1 was mixed with 2 wt. % of a synthetic diopside glass (D1) which was doped with 25 trace elements in order to give the final bulk concentrations reported in Supplementary Table S-2 (MORB1-2D1). A second basaltic glass (MORB2) with similar major element composition but directly doped with LILE was also synthesised. The remaining trace elements were added by mixing 2 wt. % of a second synthetic diopside glass (D2) to MORB2 (MORB2-2D2). In experiment PC23, a starting material prepared by mixing MORB2 with 0.4 wt. % of D1 (MORB2-DD1) was used. To each solid starting material, 1 wt. % of natural garnet seeds selected and crushed from Grytting (Norway) eclogite were added to enhance garnet growth during the experiments. Solutions with 1, 5, 10, or 15 wt. % salinity were prepared by adding pure NaCl to distilled water. For the trace element doped solutions used in the reversed experiments, equal amounts of a certified ICP standard solution for each individual trace element (1000 ppm of trace element in 5 % HNO_3) were mixed and evaporated under an infrared lamp. The solid residue was subsequently dissolved in a smaller amount of 5 % HNO_3 to obtain higher trace element concentrations and the resulting milky solution was left to rest for 1 month. After the deposition of the insoluble residue, the clear solution at the top was separated. The compositions from ICP-MS analyses of the two different doped solutions obtained with this procedure are given in Table S-2 (SOL1 and SOL2).

Experiments

For each experiment, some of the solution was pipetted into a Pt or Au capsule (5 mm outer diameter, 10 mm long, 0.2 mm wall thickness), then a layer of MORB glass powder (~ 55 mg) was added, followed by a layer of diamond powder (with 10-20 µm grain diameter). The remaining fluid was added after the diamonds to avoid suspending the first layer of basaltic starting material, which could contaminate the diamond trap. At last, another layer of MORB glass was added. The resulting total fluid/glass weight ratio ranged from 0.30 to 0.45. The capsule was weighed before and after welding of the top lid to assure that no water loss

occurred. Each capsule was also left overnight in an oven at 130 °C and weighed again to verify the sealing before the experiment. High pressure experiments were carried out at 4 GPa and 800 °C in an end-loaded piston cylinder apparatus using ½ inch MgO-NaCl assemblies with a stepped graphite furnace. Temperature was measured with a S-type (Pt/Pt-Rh) thermocouple and monitored by a Eurotherm controller. Long compression and decompression times (16-20 hours) were used to reduce capsule deformation. Temperature was raised at constant pressure after compression with a rate of 100 °C/min. In some experiments, a temperature fluctuation of ± 30 °C was applied after an initial equilibration at constant temperature for ~ 36 hours to nucleate the stable mineral assemblage. The temperature cycling was terminated ~24 hours before quenching to allow final equilibration. During temperature cycling, linear ramps in temperature (from 770 to 830 °C and back) lasted 2 hours each, with dwelling times at both temperatures of 2 hours; a single temperature cycle lasted in total 8 hours. The duration of the experiments at combined high pressure and high temperature was 2-7 days. Oxygen fugacity was not controlled, but probably was near the Ni-NiO buffer. The runs were quenched by shutting off the power at constant pressure before starting decompression.

Analytics

After the experiments, the retrieved capsules were immediately cooled in liquid nitrogen and then stored in a freezer at -18 °C until the day of the analysis. On that day, each capsule was taken out of the freezer, cooled further to -50 to -100 °C, and then cut longitudinally in half with a razor blade attached to an opening device. One half of the frozen capsule was then quickly transferred to a Laser-Ablation Inductively-Coupled-Plasma Mass-Spectrometry (LA-ICP-MS) sample chamber equipped with a Peltier-cooling element to keep the sample frozen during the entire measurement. Tests with H_2O-ethanol mixtures revealed that the temperature in this sample chamber was *ca.* -30 °C. Analysing the diamond trap in frozen state is necessary to avoid element fractionation during solution evaporation, which would introduce major uncertainties in the quantification procedure. The LA-ICP-MS measurements were performed with a 193 nm ArF GeolasPro laser ablation unit (Coherent, USA) connected to a Elan DRC-e quadrupole ICP-MS unit (Perkin Elmer, Canada). The sample chamber was flushed with He at a flow rate of 0.4 l/min, to which 5 ml/min H_2 was admixed on the way to the ICP-MS. Measured isotopes included ^{7}Li, ^{9}Be, ^{11}B, ^{23}Na, ^{25}Mg, ^{27}Al, ^{30}Si, ^{35}Cl, ^{43}Ca, ^{45}Sc, ^{49}Ti, ^{57}Fe, ^{85}Rb, ^{88}Sr, ^{89}Y, ^{90}Zr, ^{93}Nb, ^{133}Cs, ^{137}Ba, ^{139}La, ^{140}Ce, ^{146}Nd, ^{147}Sm, ^{153}Eu, ^{157}Gd, ^{163}Dy, ^{167}Er, ^{172}Yb, ^{175}Lu, ^{178}Hf, ^{181}Ta, ^{208}Pb, ^{232}Th, and ^{238}U, using a dwell time of 10 ms. The ICP-MS was tuned to a thorium oxide production rate of 0.05-0.10 % and a rate of doubly charged Ca ions of 0.15-0.25 % based on measurements on NIST SRM 610 glass (Jochum *et al*., 2011). The diamond trap layer was analysed by moving the laser beam at constant velocity along two perpendicular transects (parallel and perpendicular to the diamond layer, see Fig. 1a) using a laser spot size of 50-70 μm and a repetition rate of 7 Hz. The signals resulting from each transect (Fig. 1c) were divided into 3-4 separate integration intervals, for which element concentrations were calculated. The NIST SRM 610 glass and a well-characterised, natural afghanite crystal (Seo *et al*., 2011) were used as external standards. Chlorine (or Cs in experiments conducted with pure water) was used as internal standard, because these elements are expected to partition strongly into the fluid in the K-free eclogite-water system at the experimental conditions. Indeed, chlorine was never detected in any of the crystalline phases. Chlorine contents in the fluid phase were corrected for the dilution effect by dissolved solutes (mostly SiO_2), as determined from the diamond trap analyses. After analysis of the diamond trap, the capsules were left to evaporate at room temperature and subsequently were impregnated with epoxy resin and were polished to expose minerals for LA-ICP-MS measurements. The largest suitable spot sizes to analyse single crystals and the rims in zoned garnets were chosen, usually in the range of 7-20 μm. Averages obtained from measurements of 4 to 7 separate crystals within the capsule were used to calculate the compositions of garnet (Supplementary Table S-5), omphacite (Table S-6) and rutile (Table S-7). Special care was taken in the garnet measurements to only analyse inclusion-free rim portions and to avoid the natural garnet seeds, which showed distinctively different composition. To calculate bulk fluid/eclogite partition coefficients, first the fluid/mineral partition coefficients for each mineral were calculated, and then the results normalised to a representative eclogitic composition of 59 % omphacite, 39 % garnet and 2 % rutile.

Major element compositions of minerals were also measured by electron microprobe. A JEOL JXA 8200 instrument was used with a focused beam, an acceleration voltage of 15kV, a beam current 15nA and counting times of 10 sec on the background and 20 sec on the peak. The following standards were used: Diopside for Si, Mg, Ca; $MnTiO_3$ for Ti; Fe_2O_3 for Fe, albite for Na; corundum for Al.

Supplementary Discussion

Phase Assemblage in Experiments and in Natural MORB Eclogites

The starting material used in the experiments was designed to be very similar to that of the study of Kessel *et al*. (2005) in order to facilitate the comparison of the Cl-free experiments. In particular, as in the study of Kessel *et al*. (2005), the simplified MORB

composition used did not contain any phosphorus or potassium. This is well justified, since both P (0.184 wt. % P_2O_5) and K (0.160 wt. % K_2O) concentrations in natural MORB are very low (Gale *et al.*, 2013). Natural eclogites occasionally contain apatite and phengite, which could be important hosts for certain trace elements (REE in apatite, alkalis and Ba in phengite). However, we argue here that due to the low P and K contents of MORB, these phases will either not occur at all or only occur in insignificant traces in eclogites of MORB composition.

Konzett and Frost (2009) measured the solubility of phosphorus in garnet of MORB eclogite. They observed a solubility of P_2O_5 in the garnet phase of about 0.3 wt. % at 4 GPa. They therefore concluded that virtually all P in a MORB eclogite will be contained in garnet. If apatite is observed in MORB eclogites, it is often a secondary alteration product, *e.g.*, formed by low-temperature exsolution from garnet. This effect was already observed by Fung and Haggerty (1995); see also Keller and Ague (2019). Moreover, we note that in the presence of NaCl, apatite becomes quite soluble in aqueous fluids (Mair *et al.*, 2017), such that traces of apatite would readily be dissolved during dehydration of the basaltic crust.

The low average K_2O content of 0.16 wt. % limits the amount of phengite that may form in an eclogite of MORB composition. Therefore, typical MORB eclogites either contain no (primary) phengite at all or at most traces of this mineral. In the classical eclogite occurrences of the Bohemian Massif in central Europe, Okrusch *et al.* (1991) distinguished three lithological types, two of which do not contain any phengite. Similar, phengite-free eclogites of MORB composition were also described by Heinrich (1982), Tubia and Ibarguchi (1991), and Imayama *et al.* (2017). Eclogites from the North Dulan Belt in China, which formed from N-type and E-type MORB may or may not contain phengite; however, in every case the modal abundance is less than 1 % (Song *et al.*, 2003). Very likely, the occurrence of phengite is limited to the more K-enriched E-MORB types. Finally, we note that during interaction with an aqueous fluid, K will partition into the fluid, which should destabilise any traces of phengite.

Silica Content of Starting Materials

The silica content of the solid starting material (54 – 55 wt. %, Table S-2) is higher than in average MORB (50.47 wt. %, Gale *et al.*, 2013). This, however, compensates for the effect that in our experiments, the fluid/solid ratio is 0.3 – 0.5 and therefore much higher than in nature. These high fluid/solid ratios are necessary in order to be able to trap sufficient fluid in the diamond layer for analysis. Silica preferentially partitions into the fluid and is the most abundant solute in the aqueous phase (*e.g.*, Kessel *et al.*, 2005). This has the effect of shifting the composition of the solid residue back to that of MORB. Indeed, our experiments produce a typical eclogite phase assemblage (Fig. 1, main text) without any excess quartz or coesite.

Comparison of Trace Element Ratios in Primitive Arc Basalts With Those Observed in Experiments

Certain trace element ratios are considered to be particularly characteristic for subduction zone magmas; this includes in particular high Ba/Nb (*e.g.*, Pearce *et al.*, 2005), Ba/La (*e.g.*, Rüpke *et al.*, 2002), and U/Th ratios (*e.g.*, Bali *et al.*, 2011). Here, we compare these ratios in natural, primitive arc basalts with those predicted by our experimental data. Average primitive arc basalt compositions for 14 different subduction zones were taken from the compilation in Kelemen and Hanghøj (2005). Fluid compositions released from the basaltic oceanic crust were obtained by assuming average MORB composition for the crust (Gale *et al.*, 2013) and very low fluid/solid ratios. In this limiting case, the concentration ratio of two elements X and Y in the fluid may be estimated from the equation

$$c_X^{fluid}/c_Y^{fluid} = (c_X^{MORB}/c_Y^{MORB})\,(D_X^{fluid/eclogite}/D_Y^{fluid/eclogite})$$

These element ratios are directly given as ppm/ppm ratios; they are not normalised to MORB compositions. For Ba/Nb, the data compiled by Kelemen *et al.* (2005) span a range from 47 to 352. For fluid salinities with > 4 wt. % Cl (experiments PC27, PC36, and PC39, Table S-8), the predicted Ba/Nb ratios in the fluid range from 1280 to 3201. This means that already a small addition of such a fluid to the source of melting may produce the observed high Ba/Nb ratios. For Ba/La, the situation is similar. In average primitive arc basalts, this ratio ranges from 13 to 48, the ratio calculated for the fluid in the same three experiments as above is between 18 and 605. U/Th ratios in arc basalts are usually higher than in MORB (0.29); the average data by Kelemen *et al.* (2005) suggest a range from 0.11 to 0.65. In the fluids, the calculated ratio is between 3.1 and 5.0, indicating again that already a minor fluid addition to the source of melting will shift the ratio into the right direction. For the U/Th data, however, it has to be considered that U solubility in fluids increases with oxygen fugacity (Bali *et al.*, 2011). Oxygen fugacity in our experiments was not buffered, but is likely close to the Ni-NiO buffer. For a quantitative discussion of the effect of oxygen fugacity on U/Th ratios in subduction zone fluids, see Bali *et al*. (2011).

Supplementary Tables

Table S-1 Summary of experiments.

Experiment	NaCl in Fluid (wt. %)	Doped Fluid	Solid Starting Material	Capsule Material	Duration (h)	Temperature Fluctuations
PC09	0	-	MORB1-2D1	Au	84	no
PC22	0	-	MORB1-2D1	Pt	120	no
PC37	0	-	MORB2-2D2	Pt	68	yes
PC38	0	-	MORB2-2D2	Pt	128	no
PC14	1	-	MORB1-2D1	Au	69	no
PC23	5	-	MORB2-DD1	Pt	163	yes
PC10	10	-	MORB1-2D1	Au	68	no
PC25	10	-	MORB2-2D2	Pt	102	yes
PC27	10	-	MORB2-2D2	Pt	93	yes
PC36	15	-	MORB2-2D2	Pt	103	yes
PC39	15	-	MORB2-2D2	Pt	126	yes
PC15	15	-	MORB1-2D1	Au	63	no
PC24*	0	SOL1	MORB1	Pt	144	yes
PC18*	10	SOL2	MORB1	Pt	52	no

* reversed experiments

Table S-2 Starting material.

		MORB1	MORB1-2D1	MORB2-2D2	MORB2-DD1	SOL1	SOL2
Major elements (wt. %)	SiO_2	54.04 (18)	53.79 (19)	55.62 (17)	55.78 (15)		
	Al_2O_3	17.38 (6)	17.04 (6)	17.26 (12)	17.54 (11)		
	MgO	5.56 (3)	5.73 (3)	5.41 (3)	5.27 (2)		
	CaO	9.52 (2)	9.75 (2)	8.88 (8)	8.66 (8)		
	FeO	8.30 (12)	8.14 (13)	6.93 (5)	7.04 (6)		
	Na_2O	3.90 (2)	3.83 (3)	3.77 (9)	3.83 (8)		
Trace elements (ppm)	Li		236 (2)	1029 (16)	1076 (15)		100
	Be		192 (1)	1000 (11)	1040 (10)	202	100
	B		45 (1)	495 (16)	266 (15)	159	74
	Rb		61 (1)	777 (16)	728 (16)		99
	Cs		6.2 (1)	1077 (16)	1079 (15)	198	95
	Sr		254 (2)	1068 (7)	877 (8)	178	98
	Ba		456 (2)	1092 (4)	1145 (5)	180	98
	Ti	7718 (18)	7565 (20)	7011 (117)	7124 (115)		
	Nb		138 (1)	77.4 (6)	30.7 (2)	103	17
	Ta		75 (1)	82.0 (9)	15.2 (2)	104	8
	Zr		119 (1)	37.8 (3)	33.1 (2)	188	96
	Hf		121 (1)	38.9 (4)	24.5 (2)	186	98
	La		208 (2)	211 (2)	41.8 (4)	142	99
	Ce		818 (5)	519 (3)	562 (4)	146	99
	Nd		222 (1)	221 (2)	44.0 (2)	154	99
	Sm		215 (2)	224 (1)	42.3 (3)	164	99
	Eu		217 (2)	223 (2)	45.9 (5)	166	99
	Gd		239 (2)	248 (1)	47.2 (4)	168	98
	Dy		245 (2)	243 (3)	48.7 (5)	175	98
	Er		240 (2)	310 (4)	47.4 (4)	177	98
	Yb		241 (2)	296 (3)	47.6 (4)	174	98
	Lu		248 (3)	243 (3)	49.5 (6)	177	98
	Y		250 (3)	36.7 (3)	50.5 (7)	161	98
	Sc			261 (5)			
	Pb		92.5 (4)	530 (5)	21.1 (9)	189	97
	Th		198 (3)	106 (1)	39.4 (7)	117	26
	U		275 (2)	134 (1)	54.9 (4)	195	97

Numbers in parentheses are one standard deviation in the last digits. Total iron is given as FeO.

Table S-3 Microprobe analyses of garnet and omphacite (in wt. %).

Garnet									
SiO_2	39.17	39.32	39.86	39.43	39.25	38.77	39.02	39.19	39.26
TiO_2	0.69	0.69	0.71	0.64	0.63	0.89	0.79	0.63	0.74
Al_2O_3	22.00	21.53	21.91	21.93	21.67	20.83	21.33	21.47	20.80
MgO	7.35	7.46	7.36	7.15	7.17	7.29	6.66	8.18	6.69
CaO	11.37	10.82	10.74	10.76	10.18	9.85	11.32	8.50	10.89
FeO	20.04	20.83	21.08	20.57	21.60	22.27	21.21	22.14	21.80
Na_2O	0.06	0.06	0.05	0.09	0.06	0.07	0.09	0.06	0.21
Total	100.7	100.7	101.7	100.6	100.6	100.0	100.4	100.2	100.4

Omphacite					
SiO_2	54.57	54.69	55.81	53.81	53.53
TiO_2	0.28	0.21	0.13	0.49	0.84
Al_2O_3	12.23	12.61	10.20	10.50	10.62
MgO	7.80	8.30	9.77	8.90	8.23
CaO	12.91	12.78	14.76	13.55	13.83
FeO	4.13	3.05	5.18	7.64	6.90
Na_2O	6.01	6.52	5.81	5.46	5.90
Total	97.9	98.1	101.6	100.3	99.8

Garnet and omphacite compositions were measured on grains across the capsule in one single experiment (PC09). The average garnet composition is $(Ca_{0.29}Mg_{0.27}Fe_{0.44})_3(Al_{0.97}Fe_{0.03})_2(SiO_4)_3$, the average pyroxene composition is $Ca_{0.52}Na_{0.41}Mg_{0.46}Fe_{0.16}Al_{0.44}Si_{1.96}O_6$

Table S-4 Fluid compositions.

Experiment	PC09	PC22	PC37	PC38	PC14	PC23	PC10	PC25	PC27	PC36	PC39	PC15	PC24*	PC18*
Cl (wt. %)	0	0	0	0	0.48	2.25	3.76	3.85	4.91	6.50	6.81	6.93	0	4.23
Li	147 (8)	51.5 (9)	1172 (25)	1044 (11)	286 (15)	1322(109)	314 (14)	1468 (10)	999 (4)	987 (22)	756 (38)	564 (38)	21.6 (14)	54.1 (7)
Be	50 (3)	22.5 (3)	604 (8)	531 (9)	137 (2)	455 (32)	191 (16)	744 (4)	712 (55)	462 (14)	383 (44)	404 (29)	20.3 (16)	106 (3)
B	731 (43)	29.6 (7)	1120 (18)	1046 (14)	282 (10)	1000 (106)	2094 (224)	3668 (67)	2224 (67)	4097 (145)	2234 (201)	259 (17)	80 (5)	440 (6)
Rb	213 (9)	41.3 (3)	1529 (15)	1544 (11)	670 (42)	2266 (180)	710 (51)	5112 (89)	3089 (38)	5671 (196)	2772 (194)	394 (32)	100 (8)	314 (5)
Cs	17.0 (7)	19.3 (1)	2105 (20)	2076 (15)	51 (1)	4725 (431)	81 (6)	9912 (38)	17895 (1467)	7631 (215)	6312 (485)	125 (14)	86 (8)	427 (67)
Sr	194 (8)	90 (2)	1155 (42)	849 (15)	832 (58)	1356 (64)	396 (47)	1914 (365)	2945 (38)	2236 (167)	1235 (97)	1212 (87)	57 (5)	424 (8)
Ba	254 (23)	157 (2)	1606 (16)	1375 (22)	1285 (130)	1885 (135)	1074 (106)	2314 (4)	4542 (69)	4618 (454)	1441 (84)	2384 (173)	275 (23)	1785 (23)
Ti	162 (10)	74 (3)	387 (4)	331 (7)	280 (24)	435 (56)	414 (64)	702 (5)	272 (21)	481 (25)	367 (68)	254 (24)	133 (16)	376 (23)
Nb	10.9 (7)	4.44 (4)	17.8 (3)	14.3 (1)	19.0 (8)	4.23 (4)	27 (2)	22.7 (4)	8.5 (7)	23.3 (7)	11.7 (13)	17 (4)	0.74 (5)	3.18 (16)
Ta	0.9 (1)	0.41 (2)	3.3 (1)	2.48 (8)	2.07(14)	0.32 (1)	1.5 (2)	3.47 (2)	1.69 (5)	2.73 (12)	1.9 (3)	2.5 (2)	0.09 (2)	0.84 (14)
La	0.23 (2)	0.18 (1)	0.51 (1)	0.39 (5)	1.5 (6)	0.7 (1)	5.8 (7)	2.62 (13)	5.32 (13)	8.4 (9)	6.9 (17)	43 (2)	5.0 (4)	12.1 (6)
Ce	2.6 (2)	1.5 (2)	2.94 (7)	2.39 (14)	10 (3)	29 (5)	41 (6)	14.5 (6)	20 (1)	29.3 (18)	23 (4)	169 (7)	66 (4)	129 (6)
Nd	0.27 (3)	0.226 (4)	0.60 (3)	0.47 (4)	1.9 (8)	0.86 (10)	5.5 (3)	2.9 (4)	6.3 (4)	7.6 (11)	4.8 (11)	31.3 (17)	4.6 (4)	10.9 (6)
Sm	0.50 (5)	0.287 (8)	0.86 (4)	0.62 (2)	1.9 (6)	0.78 (7)	5.1 (11)	3.6 (5)	6.2 (4)	9.2 (13)	5.4 (8)	26.3 (17)	3.9 (3)	10.3 (3)
Eu	1.0 (1)	0.565 (5)	1.83 (3)	1.42 (3)	3.6 (1)	1.67 (23)	11.3 (13)	7.2 (9)	14.6 (9)	25 (3)	22 (5)	100 (7)	4.2 (3)	13.6 (4)
Gd	1.1 (2)	0.420 (9)	1.06 (4)	0.72 (3)	2.1 (4)	0.81 (4)	4.9 (4)	4.2 (5)	5.5 (3)	11.3 (16)	4.7 (5)	20.8 (5)	2.6 (2)	6.6 (3)
Dy	1.9 (3)	0.63 (4)	1.30 (9)	0.90 (5)	1.7 (3)	0.75 (3)	3.7 (2)	4.4 (4)	2.96 (13)	10.0 (11)	3.38 (16)	10.2 (3)	1.35 (9)	3.8 (3)
Er	1.7 (3)	0.59 (6)	1.37 (12)	0.88 (9)	1.2 (2)	0.52 (5)	2.4 (3)	4.8 (6)	1.98 (13)	8.1 (8)	3.3 (5)	6.0 (2)	1.05 (13)	4.8 (5)
Yb	1.5 (2)	0.63 (5)	1.35 (13)	0.99 (14)	1.4 (2)	0.53 (4)	2.2 (2)	5.3 (7)	2.22 (13)	6.2 (7)	4.0 (7)	5.8 (6)	1.4 (3)	7.6 (11)
Lu	1.3 (2)	0.55 (5)	0.9 (1)	0.68 (9)	1.5 (2)	0.47 (5)	1.8 (3)	4.7 (6)	1.54 (19)	4.1 (3)	3.3 (6)	5.8 (3)	1.2 (2)	9.0 (14)
Y	13 (3)	3.7 (4)	9 (2)	6.7 (17)	20 (5)	5.0 (7)	20 (4)	19 (3)	19 (3)	23 (6)	10.6 (17)	64 (20)	5.5 (6)	28 (8)
Sc			3.3 (2)	2.66 (12)				8.4 (2)	3.00 (16)	5.5 (3)	4.4 (6)			
Pb	108 (21)	17.3 (5)	371 (3)	228 (1)	177 (6)	13 (1)	589 (67)	1708 (96)	860 (109)	1428 (110)	1008 (164)	417 (28)	21.7 (11)	438 (9)
Th	0.19 (2)	0.0497 (8)	0,16 (2)	0.116 (12)	0.9 (5)	0.35 (5)	0.67 (9)	0.52 (1)	0.45 (2)	0.71 (4)	0.55 (9)	6.2 (2)	0.81 (5)	1.62 (15)
U	14 (2)	5.0 (3)	11.7 (12)	9.2 (6)	29 (2)	13.7 (16)	58 (7)	50 (2)	20 (2)	63.8 (22)	36 (6)	158 (7)	12.2 (19)	134 (13)

All compositions are given in ppm by weight, except for Cl (wt.%). Numbers in parentheses are one standard deviation in the last digits. * reversed experiments

Table S-5 Garnet compositions.

Experiment	PC09	PC22	PC37	PC38	PC14	PC23	PC10	PC25	PC27	PC36	PC39	PC15	PC24*	PC18*
Cl (wt.%) **	0	0	0	0	0.48	2.25	3.76	3.85	4.91	6.50	6.81	6.93	0	4.23
Li	< 57	22 (3)	144 (9)	113 (10)	< 188	162 (41)	< 32	112 (26)	270 (66)	76 (12)	66 (10)	124 (23)	< 39	< 69
Be	< 81	< 70	91 (28)	68 (10)	< 35	127 (32)	< 88	111 (5)	160 (37)	57 (12)	35 (3)	< 162	< 101	< 127
B	< 71	< 79	96 (11)	123 (8)	< 528	26 (1)	< 63	81 (2)	44 (2)	84 (11)	51 (6)	< 110	< 74	< 89
Rb	< 4.9	1.11 (18)	13 (9)	3.6 (5)	< 25	2.7 (7)	< 3.00	2.94 (16)	29 (12)	3.6 (0.9)	1.7 (2)	< 4.84	< 2.98	< 4.1
Cs	< 1.46	< 47	15 (11)	3.4 (5)	< 8.35	3.1 (7)	< 1.30	1.57 (12)	28 (10)	3.9 (1.6)	1.4 (2)	< 1.97	< 0.546	< 3.1
Sr	2.92 (5)	< 1.78	38 (7)	25 (6)	14 (4)	18.7 (6)	2.2 (13)	7.3 (4)	61 (11)	21 (12)	9.2 (28)	7.0 (23)	5 (1)	3.51 (14)
Ba	9.9	< 3.38	22 (12)	14 (5)	< 45.4	6.0 (5)	< 7.00	5.50 (7)	46 (29)	15 (7)	9.0 (17)	< 16	< 6.3	< 16.5
Ti	5295 (657)	4545 (517)	4251 (702)	3955 (247)	6038 (1376)	5002 (539)	5540 (521)	2998 (432)	5168 (514)	4122 (2160)	2031 (417)	4234 (372)	4486 (224)	2877 (465)
Nb	28 (3)	28 (3)	9.4 (23)	9 (3)	50 (19)	6.1 (25)	33 (7)	11 (6)	29 (3)	31 (18)	5.0 (18)	9.6 (12)	2.4 (2)	3.1 (0.4)
Ta	12.1 (18)	13 (2)	8 (3)	7.5 (23)	22 (9)	1.6 (3)	17 (5)	11 (7)	27 (3)	31 (20)	4.7 (16)	5.7 (16)	1.7 (4)	< 2.70
Zr	80 (1)	74 (6)	106 (10)	101 (9)	76 (4)	86.9 (5)	93.9 (5)	88 (3)	63 (11)	82 (17)	67 (5)	60 (4)	74 (3)	61 (3)
Hf	33 (3)	40 (2)	36 (4)	33 (4)	41 (2)	17 (3)	54 (4)	26 (2)	32 (5)	32 (7)	23 (2)	43 (4)	19 (3)	22.9 (13)
La	< 1.02	0.65 (4)	5.5 (13)	5.7 (17)	12 (2)	0.52 (8)	< 1.13	1.4 (3)	13 (3)	2.0 (0.8)	1.6 (5)	12 (5)	4.7 (1)	< 1.54
Ce	13.1 (4)	7.1 (3)	41 (9)	27 (8)	49 (28)	36 (2)	7.4 (24)	5.0 (14)	56 (12)	9 (4)	5.0 (13)	87 (29)	74 (19)	11 (5)
Nd	< 6.42	3.5 (3)	8 (2)	8.6 (11)	< 27.3	2.1 (4)	6.6 (6)	4.9 (7)	19 (3)	11 (3)	4.7 (6)	21 (5)	8.8 (4)	< 10.8
Sm	20.7 (49)	14 (3)	34 (6)	28 (4)	36 (2)	7.8 (2)	< 21.7	36 (5)	70 (7)	67 (16)	30 (3)	119 (7)	34 (4)	17.87 (8)
Eu	46 (11)	37 (7)	77 (10)	66 (7)	66 (15)	15.2 (13)	68 (1)	82 (10)	151 (14)	141 (33)	72 (9)	205 (8)	55 (8)	47 (4)
Gd	84 (16)	65 (12)	116 (17)	105 (10)	115 (27)	18 (3)	117 (9)	134 (16)	249 (25)	204 (48)	115 (15)	254 (26)	74 (10)	45 (3)
Dy	237 (6)	223 (26)	294 (35)	291 (18)	229 (10)	44 (2)	260 (7)	435 (23)	538 (56)	473 (89)	382 (52)	423 (35)	106 (26)	58 (2)
Er	361 (43)	450 (59)	529 (52)	532 (28)	362 (40)	62 (9)	340 (18)	930 (131)	781 (103)	818 (182)	872 (117)	430 (52)	106 (32)	63 (3)
Yb	470 (121)	705 (115)	608 (48)	594 (48)	527 (127)	59 (11)	354 (9)	1146 (232)	759 (110)	983 (300)	1194 (155)	378 (48)	92 (31)	60 (4)
Lu	534 (181)	826 (148)	511 (46)	491 (47)	561 (176)	59 (11)	328 (18)	1010 (219)	613 (95)	828 (270)	1088 (137)	401 (52)	86 (22)	51.5 (7)
Y	439 (14)	411 (49)	64 (6)	93 (17)	360 (27)	136 (26)	343 (10)	110 (15)	118 (11)	139 (23)	157 (30)	454 (28)	144 (16)	128 (9)
Sc			461 (37)	407 (22)				428 (29)	402 (38)	351 (79)	388 (43)			
Pb	< 3.52	< 1.8	13 (3)	7.3 (7)	< 27	1.22 (6)	4.3 (7)	5.0 (5)	14 (2)	4.8 (8)	4.9 (8)	< 9.6	2.85 (16)	< 9.0
Th	< 1.29	0.52 (5)	1.82 (21)	3.4 (5)	4.7 (3)	0.336 (9)	< 1.28	1.7 (2)	3.6 (8)	1.05 (16)	0.76 (13)	5.4 (16)	1.1 (3)	< 1.59
U	6.9 (22)	8.1 (11)	11.7 (21)	6.0 (6)	13 (5)	3.2 (5)	< 8.0	4.1 (7)	18 (2)	10 (3)	4.2 (5)	60 (9)	11.66 (2)	8.3 (2)

All compositions are given in ppm by weight, except for Cl (wt.%); numbers in parentheses are one standard deviation in the last digits. < Detection limits are reported as maximum values when element concentrations were too low to be measured; * reversed experiments; ** Cl concentrations in the fluid of the same experiment are given for reference.

Table S-6 Omphacite compositions.

Experiment	PC09	PC22	PC37	PC38	PC14	PC23	PC10	PC25	PC27	PC36	PC39	PC15	PC24*	PC18*
Cl (wt.%) **	0	0	0	0	0.48	2.25	3.76	3.85	4.91	6.50	6.81	6.93	0	4.23
Li	293 (54)	329 (10)	1461 (52)	1298 (209)	344 (28)	1812 (285)	32 (6)	1115 (43)	1463 (30)	1044 (37)	810 (13)	204 (7)	85 (2)	126 (6)
Be	204 (9)	200 (4)	921 (39)	974 (172)	276 (13)	1065 (69)	88 (5)	798 (37)	855 (16)	804 (69)	882 (41)	203 (47)	109 (18)	153 (31)
B	106 (24)	45 (3)	353 (54)	395 (81)	157 (111)	320 (74)	63 (4)	172 (6)	140 (12)	114 (10)	104 (21)	< 41	80 (24)	97 (28)
Rb	7.2 (5)	37 (2)	120 (38)	102 (32)	9 (2)	380 (85)	3.0 (2)	186 (25)	273 (19)	49 (18)	12 (2)	24 (4)	38 (11)	38 (7)
Cs	2.1 (4)	19.46 (3)	172 (55)	147 (47)	< 2.07	620 (144)	1.30 (7)	277 (40)	413 (66)	81 (28)	26 (4)	2.1 (5)	36 (12)	32 (5)
Sr	52.4 (2)	173 (6)	341 (32)	438 (115)	146 (60)	958 (268)	2.2 (13)	305 (29)	400 (20)	300 (69)	136 (19)	42 (6)	83 (29)	63 (23)
Ba	109 (15)	260 (46)	261 (39)	271 (73)	148 (65)	1193 (456)	7.0 (3)	133 (32)	248 (45)	215 (58)	100 (17)	15 (3)	169 (38)	146 (58)
Ti	< 80	1449 (37)	2711 (411)	2696 (921)	2188 (358)	2123 (110)	5540 (521)	2088 (45)	3769 (945)	2665 (305)	2747 (171)	3664 (853)	1008 (97)	1371 (209)
Nb	< 2.94	9.6 (6)	15 (6)	12 (3)	57 (26)	2.5 (3)	33 (7)	4.9 (3)	28 (7)	2.0 (8)	1.41 (14)	39 (6)	0.49 (4)	4.00 (14)
Ta	< 2.17	2.8 (3)	14 (7)	9 (3)	24 (12)	0.81 (21)	17 (5)	3.0 (2)	25 (7)	2.8 (8)	1.01 (14)	15 (3)	0.38 (11)	1.6 (3)
Zr	20 (3)	13.9 (4)	14.6 (15)	17 (4)	35 (14)	18 (3)	93.9 (5)	13.4 (9)	22 (8)	35 (12)	8.5 (4)	8.4 (13)	11.6 (4)	20 (3)
Hf	9.1 (5)	7.6 (6)	7.0 (4)	9 (2)	34 (18)	4.3 (2)	54 (4)	9.0 (5)	12 (2)	12 (4)	4.1 (5)	10.8 (16)	2.97 (2)	15 (3)
La	9 (5)	104 (6)	43 (10)	46 (18)	303 (185)	41 (9)	1.13 (6)	43 (15)	27 (2)	1.0 (1)	0.6 (2)	51 (5)	70 (44)	31 (10)
Ce	63 (24)	624 (4)	160 (35)	222 (89)	1179 (677)	963 (168)	7.4 (2.4)	141 (44)	93 (7)	4.8 (8)	2.6 (2)	273 (28)	1305 (827)	326 (68)
Nd	15 (2)	110 (3)	46 (11)	49 (20)	315 (190)	45 (10)	6.6 (06)	45 (15)	29 (3)	6.2 (1.4)	5.0 (8)	56 (5)	74 (47)	33 (12)
Sm	16 (3)	104.7 (5)	41 (10)	49 (18)	316 (201)	37 (6)	22 (4)	43 (14)	34 (2)	19 (2)	12.0 (8)	53 (8)	71 (43)	27.4 (5)
Eu	13.5 (7)	111.3 (5)	56 (13)	59 (21)	289 (176)	46 (6)	68 (1)	51 (13)	50 (4)	27 (3)	18.7 (7)	51 (4)	59 (34)	20.8 (5)
Gd	10.0 (1)	109.8 (1)	52 (12)	47 (16)	265 (161)	33 (6)	117 (9)	46 (9)	60 (6)	41 (5)	25 (2)	41 (7)	45 (27)	16 (2)
Dy	25 (11)	106 (2)	51 (12)	42 (12)	189 (113)	24 (4)	260 (7)	49 (6)	86 (16)	57 (8)	24 (2)	42 (10)	18 (8)	9.9 (7)
Er	28 (15)	100 (6)	63 (17)	46 (14)	160 (94)	19 (4)	340 (18)	61 (8)	115 (21)	60 (12)	20 (1)	38 (9)	7.5 (15)	6.4 (6)
Yb	25 (12)	96 (6)	58 (16)	47 (16)	157 (93)	16 (3)	354 (9)	55 (6)	116 (22)	38 (11)	12.4 (4)	36 (7)	7.1 (14)	10.4 (5)
Lu	25 (14)	92 (9)	46 (12)	35 (11)	139 (79)	15 (3)	328 (18)	44 (5)	92 (16)	28 (9)	9.0 (3)	32 (10)	5.3 (3)	8.4 (6)
Y	65 (34)	118 (9)	43 (15)	14 (4)	204 (112)	75 (25)	343 (10)	17 (2)	24 (4)	40 (6)	15.5 (4)	42 (10)	27 (7)	11.6 (6)
Sc			113 (12)	99 (18)				131 (6)	139 (6)	146 (8)	98 (2)			
Pb	20 (7)	33 (3)	72 (8)	57 (16)	69 (34)	3.8 (7)	4.3 (7)	219 (122)	39 (3)	14 (2)	26 (4)	5.2 (7)	30 (12)	93 (30)
Th	5.0 (22)	67.3 (5)	16 (4)	17 (7)	274 (177)	31 (9)	1.28 (4)	14 (6)	9 (1)	0.36 (4)	0.540 (25)	27 (2)	10 (6)	8.9 (9)
U	15 (5)	179 (2)	34 (7)	38 (14)	274 (177)	57 (10)	8.0 (3)	27 (9)	20 (1)	2.3 (4)	1.14 (8)	64 (6)	52 (31)	23.3 (9)

All compositions are given in ppm by weight, except for Cl (wt.%); numbers in parentheses are one standard deviation in the last digits. < Detection limits are reported as maximum values when element concentrations were too low to be measured; * reversed experiments; ** Cl concentrations in the fluid of the same experiment are given for reference.

Table S-7 Rutile compositions.

Experiment	PC09	PC22	PC37	PC38	PC14	PC23	PC10	PC25	PC27	PC36	PC39	PC15	PC24*	PC18*
Cl (wt.%) **	0	0	0	0	0.48	2.25	3.76	3.85	4.91	6.50	6.81	6.93	0	4.23
Li	< 100	< 32	< 112	< 93	< 147	< 46	< 61	< 44	< 409	< 179	< 112	< 214	< 74	< 106
Be	< 297	< 118	< 174	< 107	< 498	< 96	< 168	< 117	< 483	< 126	< 174	< 449	< 190	< 197
B	< 164	< 132	< 184	< 251	< 350	< 84	< 75	< 109	< 562	< 188	< 184	< 225	< 155	< 139
Rb	< 11	< 1.5	< 125	< 34	< 11	< 113	< 6	< 16	< 416	< 75	< 125	< 11	< 7	< 9
Cs	< 2	< 0.8	< 220	< 88	< 5	< 156	< 1.6	< 2	< 1250	< 79	< 220	< 5	< 2	< 8
Sr	< 48	< 17	< 96	< 165	< 45	< 75	< 10	< 23	< 490	< 87	< 96	< 15	< 4	< 47
Ba	< 133	< 40	< 126	< 76	< 67	< 94	< 11	< 15	< 521	< 90	< 126	< 31	< 10	< 126
Nb	10584 (608)	11863 (682)	7067 (285)	7257 (219)	10278 (344)	2475 (80)	8164 (264)	7306 (244)	7539 (227)	7226 (161)	7067 (285)	11319 (494)	1067 (43)	1611(157)
Ta	6117 (488)	6568 (523)	7363 (362)	7862 (377)	5893 (232)	1223 (32)	4072 (105)	6688 (263)	8110 (389)	7095 (364)	7363 (362)	5476 (301)	528.0 (3)	882(97)
Zr	300.8 (3)	243.3 (2)	309 (23)	341 (13)	260 (15)	341 (17)	307 (16)	401 (24)	302 (12)	331 (29)	309 (23)	346 (42)	276 (10)	274(16)
Hf	263 (16)	257 (16)	130 (23)	104 (12)	193 (41)	58 (10)	307 (52)	261 (55)	138 (16)	112 (18)	130 (23)	341 (16)	69 (20)	189(17)
La	< 7	< 14	< 6	< 38	< 37	< 3	< 36	< 10	< 20	< 4	< 6	< 4	< 7	< 122
Ce	< 69	< 104	< 27	< 147	< 307	< 129	< 172	< 51	< 74	< 9	< 27	< 6	< 123	< 1057
Nd	< 12	< 7	< 14	< 48	< 50	< 4	< 32	< 11	< 21	< 9	< 14	< 28	< 16	< 71
Sm	< 22	< 23	< 16	< 49	< 31	< 5	< 16	< 8	< 29	< 14	< 16	< 25	< 11	< 58
Eu	< 5	< 16	< 9	< 44	< 26	< 4	< 26	< 14	< 25	< 6	< 9	< 7	< 9	< 58
Gd	< 12	< 20	< 13	< 37	< 33	< 7	< 14	< 14	< 33	< 14	< 13	< 27	< 12	< 33
Dy	< 12	< 13	7	< 17	< 20	< 3	< 22	< 5	< 19	< 14	< 7	< 23	< 5	< 12
Er	< 11	< 8	< 10	< 9	< 27	< 4	< 10	< 7	< 7	< 18	< 10	< 19	< 6	< 15
Yb	< 9	< 17	< 11	< 12	< 29	< 4	< 19	< 5	< 11	< 18	< 11	< 20	< 9	< 22
Lu	< 2	< 9	< 3	< 3	< 10	< 0.8	< 11	< 2	< 7	< 9	< 3	< 6	< 4	< 4
Y	< 4	< 9	< 3	< 5	< 15	< 4	< 15	< 2	< 8	< 7	< 3	< 8	< 10	< 10
Sc			< 39	< 38				< 36	< 24	< 51	< 39			
Pb	< 17	< 3	< 39	< 34	< 35	< 5	< 13	< 16	< 216	< 54	< 39	< 18	< 6	< 33
Th	< 3	< 8	< 3	< 20	< 26	< 4	< 15	< 4	< 9	< 2	< 3	< 6	< 3	< 18
U	< 31	< 33	< 8	< 39	< 61	< 8	< 59	< 24	< 36	< 19	< 8	< 74	< 20	< 92

All compositions are given in ppm by weight, except for Cl (wt.%); numbers in parentheses are one standard deviation in the last digits. < Detection limits are reported as maximum values when element concentrations were too low to be measured; * reversed experiments; ** Cl concentrations in the fluid of the same experiment are given for reference.

Table S-8 Fluid/eclogite partition coefficients.

Experiment	PC09	PC22	PC37	PC38	PC14	PC23	PC10	PC25	PC27	PC36	PC39	PC15	PC24*	PC18*
Cl (wt.%) **	0	0	0	0	0.48	2.25	3.76	3.85	4.91	6.50	6.81	6.93	0	4.23
Li	> 0.74	0 (11)	1.25 (7)	1.27 (21)	> 1.01	1.1 (3)	> 1.7	2.06 (9)	1.01 (4)	1.50 (8)	1.48 (9)	3.3 (3)	> 0.32	> 0.52
Be	> 0.32	> 0.15	1.02 (6)	0.87 (16)	> 0.45	0.66 (8)	> 1.3	1.42 (7)	1.23 (11)	0.91 (10)	0.70 (11)	> 2.2	> 0.19	> 0.74
B	> 7.9	> 0.51	4.5 (6)	3.7 (7)	> 0.92	4.9 (16)	> 25	27 (1)	22 (2)	40 (4)	27 (6)	> 3.8	> 1.04	> 4.7
Rb	> 34	1.82 (9)	20 (6)	25 (8)	> 43	10 (3)	> 170	45 (7)	17.6 (14)	185 (73)	349 (77)	> 24	> 4.2	> 17
Cs	> 9.1	> 1.6	19 (6)	23 (7)	> 11	13 (4)	> 88	59 (9)	69 (16)	152 (55)	398 (96)	> 60	> 3.9	> 21
Sr	6.0 (3)	> 0.86	5.3 (6)	3.1 (8)	9 (4)	2.3 (7)	14 (3)	10 (3)	11.1 (7)	12 (3)	15 (3)	43 (9)	1.1 (5)	11(4)
Ba	> 3.6	> 0.99	9.7 (15)	8.2 (23)	> 12	2.6 (12)	> 112	28 (7)	27 (5)	34 (12)	23 (5)	> 153	> 2.6	> 19
Ti	> 0.075	0.0274 (17)	0.116 (8)	0.103 (12)	0.075 (10)	0.133 (13)	0.131 (15)	0.287 (13)	0.063 (7)	0.15 (3)	0.149 (19)	0.065 (8)	0.055 (5)	0.191 (18)
Nb	> 0.049	0.01748 (16)	0.116 (7)	0.092 (4)	0.073 (7)	0.079 (6)	0.154 (12)	0.148 (12)	0.047 (4)	0.148 (13)	0.078 (6)	0.069 (6)	0.033 (4)	0.089 (6)
Ta	> 0.0067	0.00294 (11)	0.021 (2)	0.015 (1)	0.015 (2)	0.0126 (16)	> 0.017	0.025 (3)	0.009 (1)	0.018 (2)	0.0130 (17)	0.020 (2)	0.0077 (16)	> 0.043
La	> 0.041	0.0028 (2)	0.018 (4)	0.013 (6)	0.0083 (78)	0.028 (10)	> 0.24	0.10 (4)	0.25 (3)	6.0 (18)	7 (3)	1.22 (18)	0.12 (8)	> 0.62
Ce	0.060 (25)	0.0041 (5)	0.026 (5)	0.017 (7)	0.014 (12)	0.049 (17)	0.27 (13)	0.17 (6)	0.25 (3)	4.4 (12)	6.3 (17)	0.85 (12)	0.08 (5)	0.64 (16)
Nd	> 0.023	0.0034 (2)	0.020 (5)	0.014 (6)	> 0.0093	0.031 (10)	> 0.22	0.10 (4)	0.25 (3)	0.9 (3)	1.0 (3)	0.74 (10)	0.10 (6)	> 0.46
Sm	0.028 (6)	0.0042 (1)	0.022 (5)	0.015 (5)	0.010 (8)	0.030 (7)	0.16 (7)	0.09 (3)	0.128 (14)	0.24 (7)	0.28 (5)	0.33 (4)	0.07 (4)	0.437 (16)
Eu	0.039 (1)	0.0069 (2)	0.028 (4)	0.023 (5)	0.018 (14)	0.050 (11)	0.23 (5)	0.114 (25)	0.161 (18)	0.34 (10)	0.56 (15)	0.89 (8)	0.07 (3)	0.43 (3)
Gd	0.029 (9)	0.0046 (3)	0.014 (2)	0.010 (2)	0.010 (7)	0.030 (5)	0.071 (11)	0.052 (10)	0.040 (5)	0.11 (3)	0.076 (14)	0.165 (18)	0.045 (15)	0.242 (21)
Dy	0.017 (3)	0.0041 (4)	0.0088 (14)	0.0064 (7)	0.008 (4)	0.023 (2)	0.032 (3)	0.021 (3)	0.0111 (14)	0.045 (12)	0.020 (3)	0.053 (5)	0.025 (7)	0.129 (11)
Er	0.010 (3)	0.0025 (4)	0.0055 (9)	0.0037 (5)	0.0050 (17)	0.014 (3)	0.017 (3)	0.012 (3)	0.0052 (9)	0.022 (7)	0.009 (2)	0.031 (4)	0.022 (9)	0.166 (21)
Yb	0.007 (3)	0.0019 (4)	0.0048 (8)	0.0037 (8)	0.0047 (16)	0.016 (3)	0.0152 (18)	0.011 (3)	0.006 (1)	0.015 (6)	0.008 (2)	0.033 (7)	0.033 (16)	0.25 (4)
Lu	0.006 (3)	0.0014 (3)	0.0037 (7)	0.0032 (7)	0.0048 (018)	0.014 (3)	0.0129 (25)	0.011 (4)	0.005 (1)	0.012 (5)	0.008 (2)	0.032 (6)	0.031 (13)	0.35 (5)
Y	0.062 (5)	0.016 (3)	0.18 (6)	0.15 (6)	0.07 (3)	0.049 (14)	0.13 (3)	0.35 (9)	0.30 (6)	0.29 (9)	0.15 (5)	0.31 (10)	0.075 (14)	0.47 (15)
Sc			0.0131 (14)	0.0120 (11)				0.033 (2)	0.0123 (13)	0.024 (4)	0.021 (4)			
Pb	> 8.1	> 0.84	7.6 (9)	6.1 (16)	> 3.4	4.7 (10)	> 64	13 (8)	30 (5)	142 (29)	58 (16)	> 60	1.1 (5)	> 7.3
Th	> 0.053	0.00123 (3)	0.015 (5)	0.010 (5)	0.01 (1)	0.019 (8)	> 0.043	0.06 (2)	0.064 (9)	1.12 (16)	0.88 (17)	0.33 (4)	0.12 (8)	> 0.27
U	1.2 (5)	0.045 (3)	0.47 (12)	0.37 (014)	0.17 (12)	0.39 (11)	1.9 (9)	2.8 (9)	1.04 (14)	12 (3)	15 (3)	2.5 (3)	0.34 (22)	7.8 (9)

Numbers in parentheses are one standard deviation in the last digits; > minimum values of D are reported when only maximum concentrations of trace elements were available for garnet and/or omphacite.; * reversed experiments; ** Cl concentrations in the fluid of the same experiment are given for reference.

Supplementary Information References

Fung, A.T., Haggerty, S.E. (1995) Petrography and mineral compositions of eclogites from the Koidu kimberlite complex, Sierra-Leone. *Journal of Geophysical Research* 100, 20451-20473.

Gale, A., Dalton, C.A., Langmuir, C.H., Su, Y.J., Schilling, J.G. (2013) The mean composition of ocean ridge basalts. *Geochemistry Geophysics Geosystems 14*, 489-518.

Heinrich, C.A. (1982) Kyanite-eclogite to amphibolite facies evolution of hydrous mafic and pelitic rocks, Adula-Nappe, Central Alps. *Contributions to Mineralogy and Petrology* 81, 30-38

Imayama, T., Oh, C.W., Baltybaev, S.K., Park, C.S., Yi, K., Jung, H. (2017) Paleoproterozoic high-pressure metamorphic history of the Salma eclogite on the Kola Peninsula, Russia. *Lithosphere* 9, 855–873.

Jochum, K.P. *et al.* (2011) Determination of reference values for NIST SRM 610-617 glasses following ISO guidelines. *Geostandards and Geoanalytical Research* 35, 397-429.

Keller, D.S., Ague, J.J. (2019) Crystallographic and textural evidence for precipitation of rutile, ilmenite, corundum, and apatite lamellae from garnet. *American Mineralogis*t 104, 980-995.

Mair, P., Tropper, P., Harlov, D.E., Manning, C.E. (2017) The solubility of apatite in H_2O, KCl-H_2O, NaCl-H_2O at 800 °C and 1.0 GPa: Implications for REE mobility in high-grade saline brines. *Chemical Geology* 470, 180-192.

Pearce, J.A., Stern, R.J., Bloomer, S.H., Fryer, P. (2005) Geochemical mapping of the Mariana arc-basin system: Implications for the nature and distribution of subduction components. *Geochemistry Geophysics Geosystems* 6, Article Number: Q07006.

Rüpke, L.H., Phipps Morgan, J., Hort, M., Connolly, A.D. (2002) Are the regional variations in Central American arc lavas due to differing basaltic versus peridotitic slab sources of fluids? *Geology* 30, 1035–1038.

Seo, J.H., Guillong, M., Aerts, M., Zajacz, Z., Heinrich, C.A. (2011) Microanalysis of S, Cl, and Br in fluid inclusions by LA-ICP-MS. *Chemical Geology* 284, 35-44.

Song, S., Yang, J., Liou, J.G., Wu, C., Shi, R., Xu, Z. (2003) Petrology, geochemistry and isotopic ages of eclogites from the Dulan UHPM Terrane, the North Qaidam, NW China. *Lithos* 70, 195– 211.

Tubia, J.M., Ibarguchi, J.I.G. (1991) Eclogites of the Ojén nappe: a record of subduction in the Alpujárride complex (Betic Cordilleras, southern Spain). *Journal of the Geological Society of London 148, 801-804.*